Application of the Luenberger Observer to the Sensorless Speed Control of an Induction Motor Drive: Analysis and Implementation

Gilberto Costa Drumond Sousa Ana Paula de Sá Santos Rabello

Federal University of Espírito Santo
Electrical Engineering Department
C. P. 01-9011
29060-970 Vitória – Espírito Santo – Brazil
Phone: +55.27.335.2699 Fax: +55.27.335.2650
e-mail: g.sousa@ele.ufes.br

***Abstract* - This paper discusses the analysis and implementation of a Luenberger observer applied to the estimation of the speed of an induction machine (IM) for an indirect vector control (IVC) system, operating at both low and high speeds, with and without load torques. A complete description of the technique is provided, along with some insightful explanation of their adaptation mechanism. The paper also discusses the influence of parameter variation as well as the choice of the integration routine on system dynamic and steady state characteristics.**

I. Introduction

Sensorless vector control has been a topic of interest for drive systems researchers in recent years. The advantages of substituting the mechanical sensor, usually a pulse encoder, for speed estimators are well known:

- The sensor is fragile and sensitive to hostile environments, usually present in industrial plants;
- The installation of a speed or position sensor requires a shaft extension in the machine, what adds cost to the system;
- The sensor is also expensive, sometimes costing more than the main machine;

Several techniques have been proposed in the literature for estimating the speed of an induction machine (IM). The methods can be broadly classified in two main categories: back emf methods, that derive the speed signal from the fundamental stator and current signals, and spectral analysis methods, that utilizes the natural (intrinsic) slot harmonics or intentionally injects high frequency harmonics in the machine (superimposed to the fundamental signal) to detect rotor position and speed, based on intrinsic or induced machine asymmetries.

While the techniques based on back emf do not continuously operate at zero speed, and usually presents instability problems at low speed, they are in general less demanding in terms of computational load than the techniques based on spectral analysis. Furthermore, they do not require any machine modification, what makes them suitable for application to low cost, off the shelf induction motors .

Among the several back emf methods, one technique has emerged as most promising, namely the Luenberger observer [1]. It is relatively simple to implement, and possesses good dynamic and steady state characteristics. In fact, H. Kubota et al. [2] applied the Luenberger observer to a direct vector-controlled IM drive, where the observer poles are dynamically changed to take into account the non-linear characteristics of the IM. They, however, did not fully take advantage of the potential of the technique, simplifying their implementation by forcing the observer gain matrix to zero.

II. Speed Observer Structure

The overall system block diagram is shown in Fig. 1. It consists of an IVC system where the speed sensor has been replaced for a speed estimator, based on the Luenberger observer, that produces a speed estimate from the stator voltages and currents.

If stator current ($\vec{i}_s$) and rotor flux ($\vec{\psi}_r$) are selected as state variables [2], the IM state equations in the stationary reference frame can be written as in (1), while the output equation, stator current, is given by (2):

$$\frac{d}{dt}\begin{bmatrix}\vec{i}_s\\ \vec{\psi}_r\end{bmatrix}=\begin{bmatrix}A_{11} & A_{12}\\ A_{21} & A_{22}\end{bmatrix}\begin{bmatrix}\vec{i}_s\\ \vec{\psi}_r\end{bmatrix}+\begin{bmatrix}B_1\\ 0\end{bmatrix}\vec{v}_s = A\vec{x}+B\vec{v}_s \qquad (1)$$

$$\vec{i}_s = C\vec{x} \qquad (2)$$

where:

$\vec{i}_s=\begin{bmatrix}i_{ds} & i_{qs}\end{bmatrix}^T$ is the stator current vector;

$\vec{\psi}=\begin{bmatrix}\psi_d & \psi_q\end{bmatrix}^T$ is the rotor flux vector;

$\vec{v}_s=\begin{bmatrix}v_{ds} & v_{qs}\end{bmatrix}^T$ is the applied stator voltage vector.

$$A_{11}=-\left\{\frac{R_s}{\sigma L_s}+\frac{1-\sigma}{\sigma\tau}\right\}\boldsymbol{I}=\mathrm{a}_{\mathrm{r}11}\boldsymbol{I}$$

$$A_{12}=\frac{L_m}{\sigma L_s L}\left\{\frac{1}{\tau}\boldsymbol{I}-\omega_{\mathrm{r}}\boldsymbol{J}\right\}=a_{12}\boldsymbol{I}+a_{i12}\boldsymbol{J}$$

$$A_{21}=\frac{L_m}{\tau_r}\boldsymbol{I}=a_{r21}\boldsymbol{I}$$

$$A_{22}=-\frac{1}{\tau_r}\boldsymbol{I}+\omega_{\mathrm{r}}\boldsymbol{J}=a_{r22}\boldsymbol{I}+a_{i22}\boldsymbol{J}$$

$$B_1=\frac{1}{\sigma L_s}\boldsymbol{I}=b_1\boldsymbol{I}$$

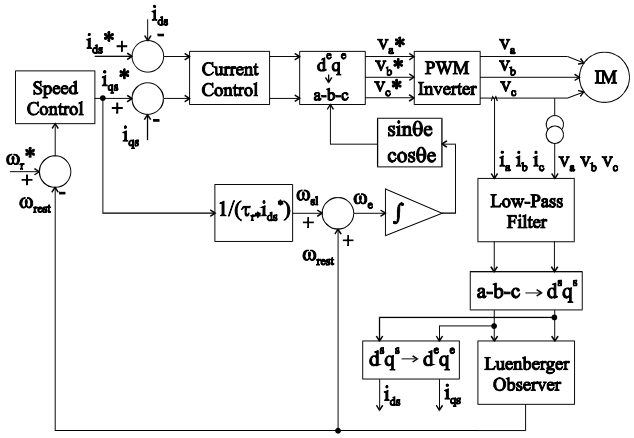

Fig. 1 - Block diagram of the proposed system.

$$C = \begin{bmatrix} \boldsymbol{I} & 0 \end{bmatrix} \qquad \boldsymbol{I} = \begin{bmatrix} 1 & 0 \\ 0 & 1 \end{bmatrix} \qquad \boldsymbol{J} = \begin{bmatrix} 0 & -1 \\ 1 & 0 \end{bmatrix}$$

R_s, R	stator and rotor resistance
L_s, L_r	stator and rotor self inductance
L_m	mutual inductance
σ	leakage coefficient, $\sigma = 1 - L_m^2 / (L_s L_r)$
τ_r	rotor time constant, $\tau_r = L_r / R_r$
ω_r	motor angular velocity

A state observer for stator current and rotor flux estimation can be derived from (1), as shown below:

$$\frac{d}{dt}\hat{\vec{x}} = \hat{A}\hat{\vec{x}} + B\vec{v}_s + G(\hat{\vec{i}}_s - \vec{i}_s) \tag{3}$$

where G is an observer gain matrix, designed to ensure a stable operation for the observer.

The observer structure can be seen on Fig. 2. It essentially duplicates the dynamics of the IM, but also possesses a corrective term contributed by the observer gain matrix G. This is necessary to reduce the sensitivity to machine and observer parameter mismatches.

In order to derive the adaptive scheme [2], Lyapunov's theorem is utilized. From (1), (2) and (3), the estimation error of the stator current and rotor flux is described by the following equation:

$$\frac{d}{dt}e = (A + GC)e - \Delta A\hat{x} \tag{4}$$

where:

$$e = x - \hat{x}\,,\ \Delta A = \hat{A} - A = \begin{bmatrix} \boldsymbol{0} & \dfrac{-\Delta\omega_r J}{c} \\ \boldsymbol{0} & \Delta\omega_r J \end{bmatrix},$$

$$c = \frac{\sigma L\ L_r}{L}\text{, and } \Delta\omega_r = \hat{\omega}_r - \omega_r$$

Now the following Lyapunov function candidate is defined:

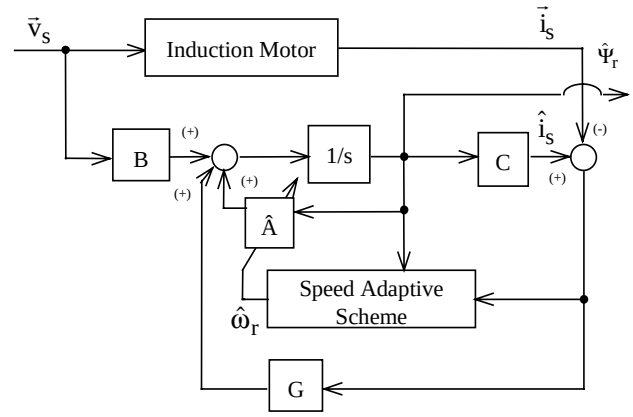

Fig. 2 - Block diagram of adaptive speed observer [2].

$$V = e^T e + \frac{(\hat{\omega}_r - \omega_r)^2}{\lambda} \tag{5}$$

where λ is a positive constant.

The time derivative of V becomes:

$$\begin{aligned} \frac{d}{dt}V = {} & e^T\left[(A + GC) + (A + GC)^T\right]e - \\ & - 2\Delta\omega_r \frac{ei_{ds}\hat{\psi}_{qr} - ei_{qs}\hat{\psi}_{dr}}{e} + \\ & + \frac{2}{\lambda}\Delta\omega_r \frac{d}{dt}\hat{\omega}_r \end{aligned} \tag{6}$$

where: $ei_{ds} = i_{ds} - \hat{i}_{ds}$ and $ei_{qs} = i_{qs} - \hat{i}_{qs}$

From (6), we can find the following adaptive scheme for the speed estimation by equalizing the second term to the third term:

$$\frac{d}{dt}\hat{\omega}_r = \frac{\lambda}{c}\left(ei_{ds}\hat{\psi}_{qr} - ei_{qs}\hat{\psi}_{dr}\right) \tag{7}$$

If the observer gain matrix G is designed so that the first term of (6) can be negative-semidefinite, the proposed speed adaptive flux observer is stable.

The motor speed can change quickly. Therefore, the following proportional and integral adaptive scheme is used in practic to improve the response of the sped estimation.

$$\hat{\omega}_r = k_P\left(ei_{ds}\hat{\psi}_{qr} - ei_{qs}\hat{\psi}_{dr}\right) + k_I\int\left(ei_{ds}\hat{\psi}_{qr} - ei_{qs}\hat{\psi}_{dr}\right) \tag{8}$$

where k_P and k_I are the arbitrary positive gain.

The observer gain matrix G is calculated by the following equation so that the observer poles are proportional to those of the induction motor (with proportionality constant $k \geq 1$):

$$G = \begin{bmatrix} g_1 & g_2 & g_3 & g_4 \\ -g_2 & g_1 & -g_4 & g_3 \end{bmatrix}^T \tag{9}$$

where:

$$g_1 = (k-1)\cdot(a_{r11} + a_{r22})$$
$$g_2 = (k-1)\cdot a_{i22}$$
$$g_3 = (k^2-1)\cdot(c\cdot a_{r11} + a_{r21}) - c\cdot(k-1)\cdot(a_{r11} + a_{r22})$$
$$g_4 = -c\cdot(k-1)\cdot a_{i22}$$

In short the adaptive system consists of a PI controller that acts upon an error signal (U) obtained as the vector product of the stator current error vector and the estimated rotor flux vector , as indicated by 10.

$$U = ei_{ds} * \hat{\Psi}_{qr} - ei_{qs} * \hat{\Psi}_{dr} \qquad (10)$$

In fact, by using the standard steady state T model for the IM (not shown), along with the phasor diagram of Fig. 3, the behavior of the error signal can be illustrated, here for a particular condition, where the system is operating at steady state at 900 rpm, and 50% of load torque. The actual speed signal is used for both vector orientation and speed control. When the speed estimate is smaller than the actual value ($\omega_{rest} < \omega_r$)(ω_{rest} = 850 rpm), the slip frequency estimate becomes greater than the correct value ($\omega_{slest} > \omega_{sl}$), causing an increase in the q-axis component, such that the estimated current vector ($\vec{\hat{i}}_{s850}$) leads the actual value ($\vec{i}_s$). As can be seen in Fig. 3, the current error vector ($e\vec{i}_{s850}$) lags the rotor flux estimate vector, such that the error given by (10) results positive. As a consequence, the PI controller increases the speed estimate until the error is driven to zero, where the speed estimate equals the actual machine speed. Opposite behavior occurs when the speed estimate is greater than the actual value, what is also illustrated in Fig. 3 for ω_{rest} = 950 rpm and vectors $\vec{\hat{i}}_{s950}$ and $e\vec{i}_{s950}$.

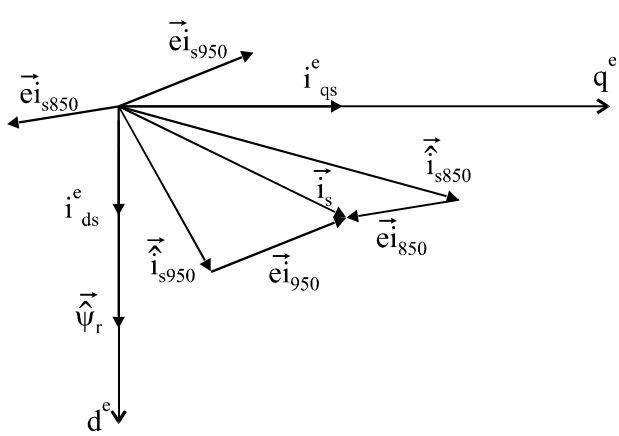

Fig. 3 - Phasor diagram of adaptive system.

III. Simulation Studies

The system was initially validated by simulation studies, using SIMNON language. A complete IVC speed control system was constructed, using a sinusoidal PWM inverter model to ensure realistic results, as shown in Fig. 4. Low-pass filters (LPF) were utilized to condition the current and voltage signals needed for the observer, as well as for the current control loop, implemented in the synchronous frame.

The system was initially tested for a 0 to 900 rpm speed reference step, followed by a load torque step of 0.5 pu. Fig. 5(a) shows reference and actual speed responses, while Fig. 5(b) presents the speed estimate along with the actual speed. The current loop operation can be observed in Fig. 5(c) and (d), for q-axis and d-axis components, respectively.

The effects of switching frequency, as well as the integration technique, on speed estimate accuracy were next investigated. Figure 6 shows a steady-state operation at 900 rpm, and 0.5 pu of load torque, when estimated speed is used in the speed control loop. For a 5 kHz PWM switching frequency, Fig. 6(a) shows a 6 rpm estimation error. This value is reduced to 3 rpm, when the switching frequency is increased to 10 kHz. Figure 6.1 shows a 5 kHz switching frequency operation, but now a trapezoidal rule of integration is used, in contrast to rectangular ruler (Euler) utilized in the previous cases. The estimation error is now reduced to 1 rpm. Due to its superior performance, trapezoidal rule was also utilized in the experimental study.

As the IM parameter are subject to change due to temperature and saturation effects, a sensitivity study was carried out, as indicated in Fig. 7.

Fig. 7(a) indicates that rotor resistance variation is a dominant factor in speed estimate accuracy, particularity at high load torques. The influence of stator resistance variation is also affected by load torque, but its impact is higher at low speeds due to a smaller back emf, Fig. 7(b). The leakage inductance variation is a secondary factor in speed estimate precision, as indicated in Fig. 7(c). It is also easier to compensate for, due to the a priori knowledge of its behavior with respect to total stator current.

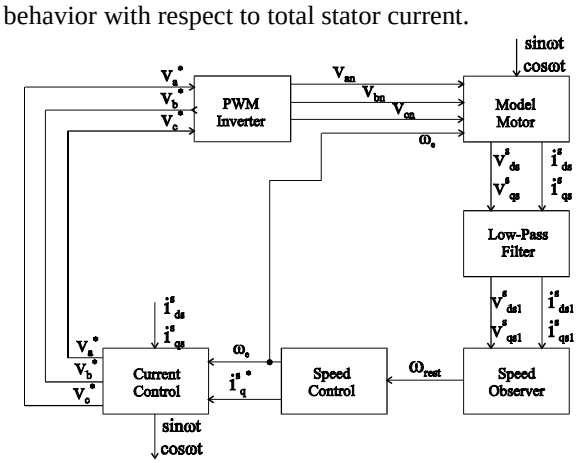

Fig. 4 - Block diagram used for simulation.

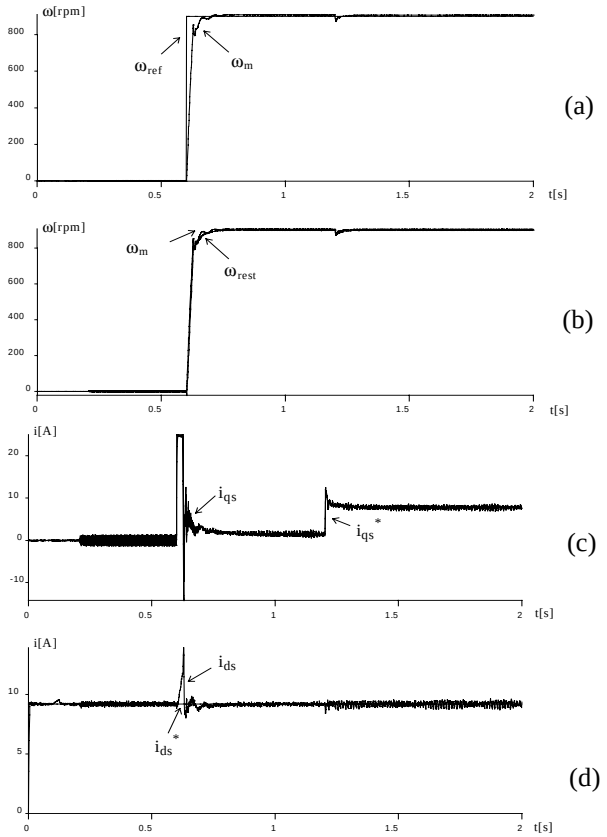

Fig. 5 - (a) reference speed (ω_{ref}) and actual speed (ω_m), (b) actual speed and estimated speed (ω_{rest}), (c) reference (i_{qs}^*) and actual (i_{qs}) q^e-axis current, (d) reference (i_{ds}^*) and actual (i_{ds}) d^e-axis current.

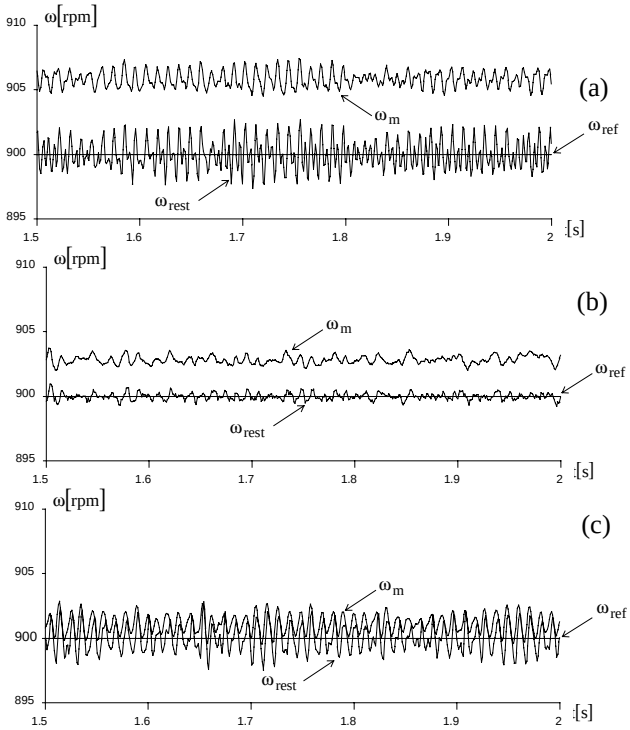

Fig. 6 – Steady state operation for 0.5 pu load torque
(a) 5kHz switching frequency, Euler method of integration;
(b) 10kHz switching frequency, Euler method of integration;
(c) 5kHz switching frequency, trapezoidal method of integration.

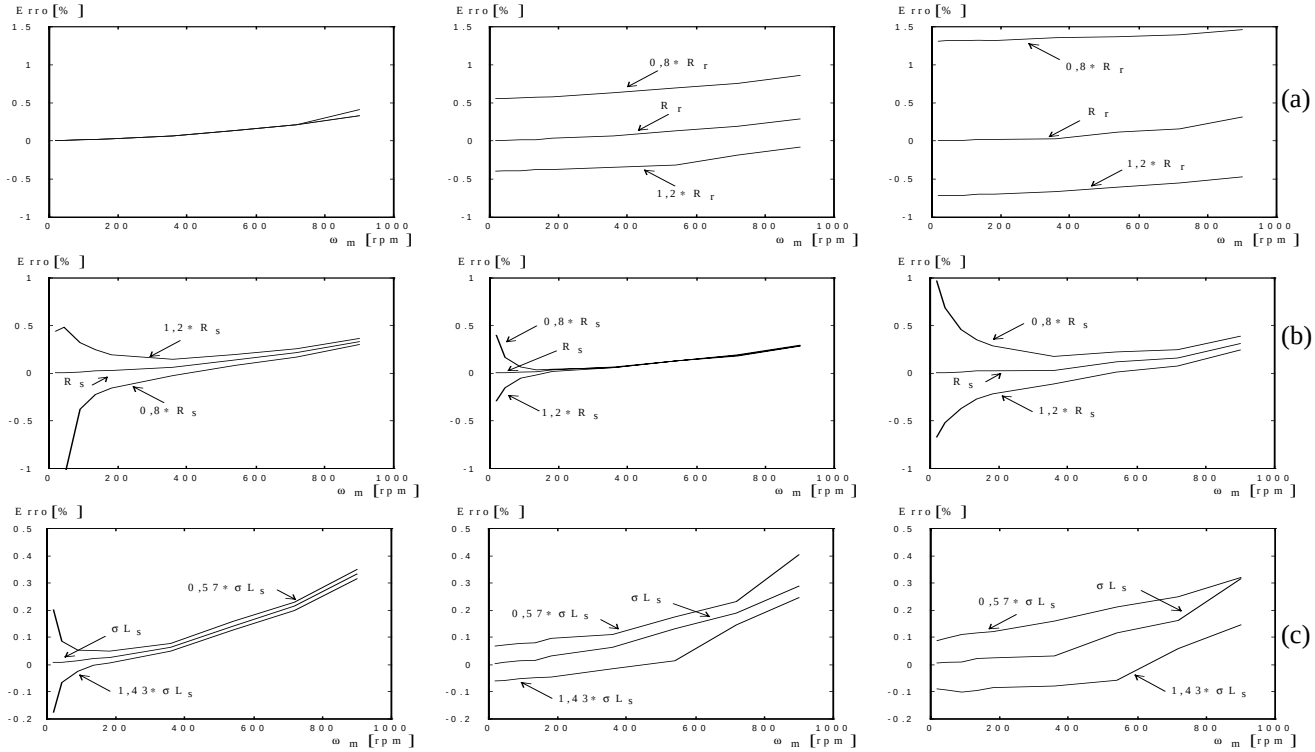

T_L = 0 pu T_L = 0,5 pu T_L = 1 pu

Erro [%] = (ω_m [rpm] - ω_{rest} [rpm]) * 100[%] / 1800 rpm

Fig.7 – Parameter variation effect on speed estimate.

IV. EXPERIMENTAL STUDIES

An actual system was next implemented, as shown in Fig. 8. It utilizes a Host PC with an embedded Texas Instrument's TMS320C25 DSP based control board from Dalanco Spry [3][4]. Except for the A/D and D/A converter, all control functions are implemented with a 200 μs sampling time. The man-machine interface is implemented in the Host PC, that is responsible for starting / stopping the system, establishing the speed reference, as well as capturing the system internal variables and graphically displaying them.

Experimental step response from 900 to 1350 rpm are shown in Fig. 9 for a 5 hp, 4 poles induction motor drive, with an inertial load of 0.057 kg*m^2. The actual and estimated speed signals agree quite well for both steady state and transient condition, good accuracy was obtained for this condition.

Four quadrant operation is illustrated in Fig. 10. The system was initially operating at 50 rpm, when the speed reference was changed to 200 rpm. After nearly 1 sec, the speed reference is set to -200 rpm, and, finally to zero. It can be seen that some spikes are present in the speed estimate, during the initial transients, and they were found to be caused by delays introduced by the LPF, and are not easy to circumvent. The q^e-axis current response is also shown in Fig. 10(c) and (d). Current oscillations are a consequence of estimate speed fluctuations. One remarkable feature is the stable operation of the system at zero speed albeit some inaccuracies in the estimate.

The impact of a sudden load step (of 0.5 pu) can be observed in Fig. 11. Good disturbance rejection can be obtained, as indicated in Fig. 11(a). Observer error (Fig. 11 (b)) is clearly noisier at higher current levels, what is propagated to speed estimate. Finally, it can be seen that IM flux is also affected by load torque, and this is attributed to a mismatch between the actual parameters, and those utilized in the observer, as well as in the slip gain, particularly the rotor time constant.

Some oscillations in the steady state condition are caused by the inverter dead time of 3μs, that has not been compensated for.

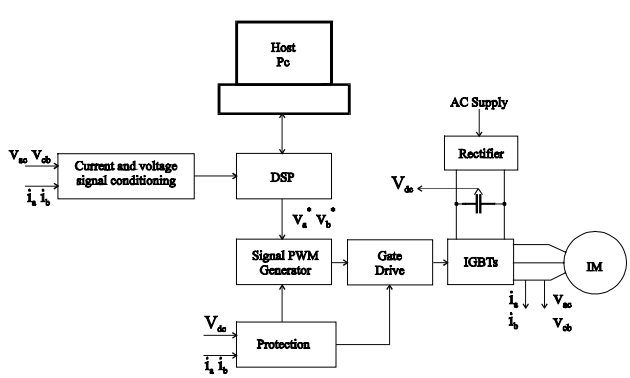

Fig. 8 - Block diagram of experimental system.

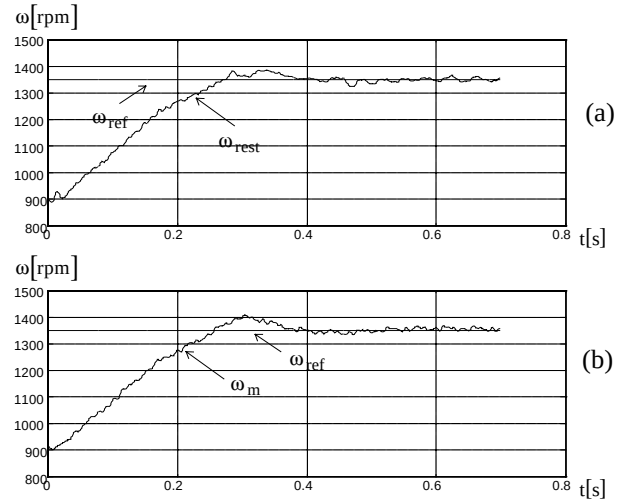

Fig. 9 - Step response to a 900 to 1350 rpm variation in reference sped, at no load:

(a) Estimated speed ($\hat{\omega}_r$) and reference speed(ω_{ref});

(b) Actual speed (ω_m) and reference speed (ω_{ref}).

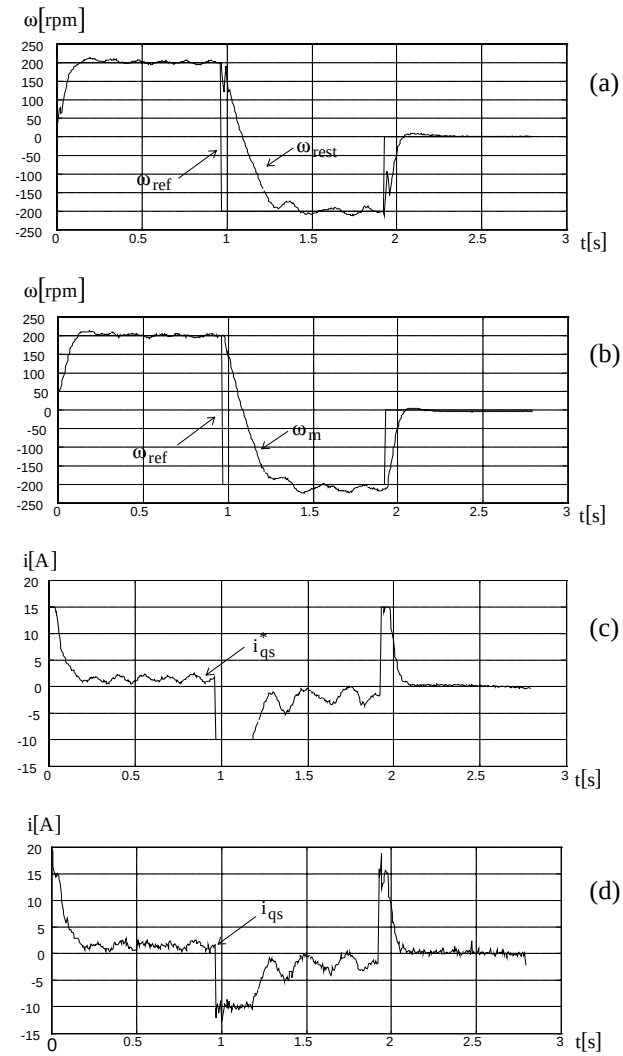

Fig. 10 - Four quadrant operation at no load:

(a) Estimated speed ($\hat{\omega}_r$) and reference speed (ω_{ref});

(b) Actual speed (ω_m) and reference speed (ω_{ref});

(c) Synchronous frame (q^e) reference current (i^*_{qs});

(d) Actual q^e-axis current (i_{qs}).

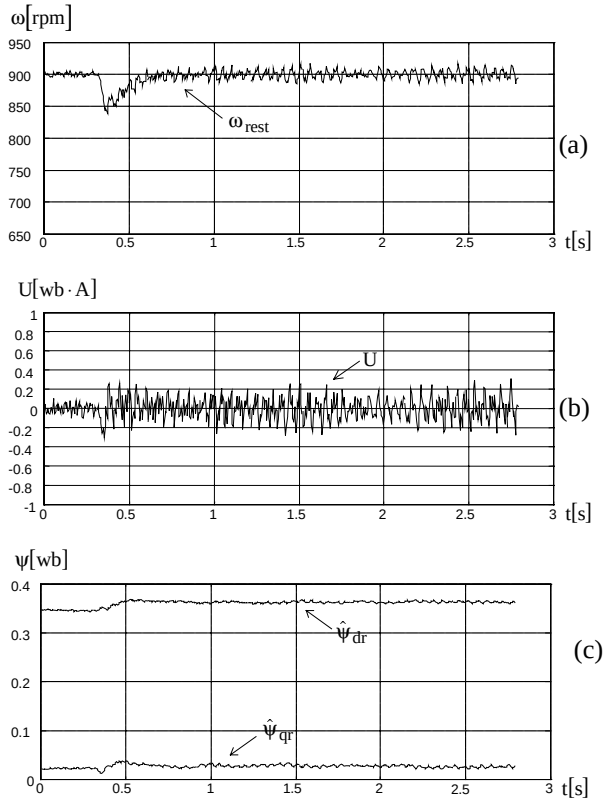

Fig. 11 - Load step (0.5 pu) response at 900 rpm operation:
(a) Estimated speed ($\hat{\omega}_r$);
(b) Observer error (U);
(c) Synchronous frame (q^e) estimated flux ($\hat{\psi}_{qr}$ e $\hat{\psi}_{dr}$).

V. Conclusion

The paper discussed the application of the Luenberger Observer to the speed estimation of an IM under indirect vector control. An insightful explanation of the adaptation mechanism was introduced, along a detailed simulation and experimental study.

The results obtained indicate that this is a viable, reasonably simple to implement technique for speed estimation of the IM, and applicable to vector control systems operating in all speed regions.

VI. Acknowledgment

The authors would like to express their gratitude to the Council of Science and Technology of Vitória (FACITEC) for its financial support for this project.

VII. References

[1] Eliane Patrício Machado Pedrini, *"Um Estudo Comparativo de Técnicas de Estimação da Velocidade do Motor de Indução Baseadas na Força Contra-Eletromotriz"*, Master's Dissertation, Federal University of Espírito Santo, 1998.

[2] H. Kubota, K. Matsuse and T. Nakano, "DSP - Based Speed Adaptive Flux Observer of Induction Motor", *IEEE Transactions on Industry Applications*, vol. 29, nº 2, pp.344 -348, 1993.

[3] *TMS320C2X User's Guide*, Texas Instruments Inc., 1990.

[4] Dalanco Spry Model 250, *Data Acquisition and Signal Processing Board Documentation*, 1990.

[5] C. Ilas, A. Bettini, L. Ferraris, G. Griva and F. Profumo, "Comparison of Different Schemes without Shaft Sensors for Field Oriented Control Drives", *Proceedings of The International Conference on Industrial Eletronics, Control and Instrumentation - IECON'94*, pp.1579 - 1588, 1994.

[6] L. A. S. Ribeiro, C. B. Jacobina e A. M. N. Lima, "Estimação da Velocidade da Máquina Assíncrona Em Acionamentos Estáticos. Parte I: Revisão e Classificação", *Congresso Brasileiro de Eletrônica de Potência - COBEP'97*, pp. 486-497, 1997.